Design Criteria for a Push-On Push-Off MEMS Bistable Device

Hen-Wei Huang, *Member, IEEE*, Fu-Wei Lee, and Yao-Joe Joseph Yang, *Member, IEEE*

***Abstract*— In this paper, we present closed-form design criteria for a microelectromechanical system push-on push-off bistable device. The design criteria, which were derived analytically, are expected to be useful for designers for rapidly designing devices with bistability and the push-on push-off capability. The aforementioned bistable device consists of a V-beam actuator, two sets of double-curved beams, and a lever connecting the two sets of beams. Spring stiffness ratio was derived as a criterion for determining the existence of bistability. The ratio between the long and the short arms of the lever was derived as the other criterion, and it was intended to be used for determining the conditions for push-on and push-off capabilities. Both criteria can be explicitly expressed in terms of the device dimensions and material properties. The derived design criteria were validated by experimental measurement results obtained for more than 100 different devices. [2015-0122]**

***Index Terms*— Bistable mechanism, lever, push-on push-off, V-beam actuator.**

I. Introduction

MICROELECTROMECHANICAL (MEMS) bistable devices [1]–[7] have been attracting attention over the past decades because they have many applications; for example, they could be used in microrelays [8], [9], microvalves [10], [11], microswitches [12], optical MEMS devices [13], and biomedical microdevices [14]. The advantages of MEMS bistable mechanisms include zero power consumption at a stable position, a quick snapping response, and a large switching displacement.

Mechanically bistable *push-on push-off* mechanisms, such as the mechanism used in a retractable ballpoint pen, are common in daily life. Devices based on this type of mechanisms, which require only one actuator (single input power source) for switching between two stable positions, can be easily realized by assembling several discrete mechanical parts. However, MEMS devices with untethered or unanchored components (i.e., discrete components) are difficult to assemble, and their operations are not reliable because of problems related to contact and friction. Therefore, the movable components of a MEMS device are typically designed as suspended compliant structures anchored on a substrate, and they are monolithically formed during manufacture. Accordingly, typical mechanical push-on push-off mechanisms commonly encountered, such as the mechanism of a retractable ballpoint pen, have not been successfully realized in MEMS devices with *reliable* and *durable* performance.

In [15], we presented the first fully compliant MEMS push-on push-off bistable device that required only one actuator for full operation. The proposed device can be easily realized on a silicon-on-insulator wafer by using standard inductively coupled plasma reactive-ion etching and a single photomask. Because the proposed device required only one actuator and was monolithically fabricated, it offered several advantages: it involved a simple operation, and a simple fabrication process; required a single driving power source; and showed low system complexity, reliable performance, and high durability. Although the operation and functionality of the proposed device were described in [15] (with animations), detailed modeling of the device and the criteria to be used in its design have yet to be presented. In this paper, we present the design criteria of the push-on push-off microdevice. The first design criterion provides conditions for determining device bistability, and the second design criterion presents conditions that can be used for ensuring the push-on push-off capability. Both criteria were derived analytically and are in closed form. Experimental measurement results for more than 100 devices of different dimensions are presented to validate the analytical derivations of both criteria.

II. Device Operation and Behavior

As shown in Fig. 1(a), the push-on push-off device consists of two curved-beam structures [16] and one V-beam actuator (VBA) [17]. One curved beam serves as the bistable switch mechanism (BSM), and the other curved beam serves as the displacement amplifying mechanism (DAM). A lever is connected to the right ends of the BSM and DAM. Fig. 1(b) shows the SEM picture of the push-on push-off bistable device. With a single photomask, the proposed device can be easily realized by using an approach which is commonly used for create high-aspect-ratio movable microstructures [18]. This approach employs inductively coupled plasma reactive-ion etching (ICP-RIE) process on a silicon-on-insulator (SOI) wafer. All the movable parts of the device are suspended structures anchored at the substrate, the operation of the device is quite smooth and reliable.

Fig. 1(c) illustrates the push-on transition. When a DC input voltage is applied on the VBA, the end displacement of the DAM (d_{DAM}) causes the transverse displacement (D_{DAM}) of the central point. When d_{DAM} is greater than a certain value $d_{DAM-push-on}$, D_{DAM} is sufficiently large to push the BSM

Manuscript received May 3, 2015; revised April 7, 2016; accepted May 20, 2016. Date of publication August 12, 2016; date of current version September 29, 2016. This work was supported by the National Science Council, Taiwan, within the Ministry of Science and Technology under Contract NSC 100-2221-E-002-075-MY3. Subject Editor C. Mastrangelo.

The authors are with the Department of Mechanical Engineering, National Taiwan University, Taipei 10617, Taiwan (e-mail: victor1233@mems.me.ntu.edu.tw; fuweilee1221@mems.me.ntu.edu.tw; yjy@ntu.edu.tw).

Color versions of one or more of the figures in this paper are available online at http://ieeexplore.ieee.org.

Digital Object Identifier 10.1109/JMEMS.2016.2574874

1057-7157 © 2016 IEEE. Personal use is permitted, but republication/redistribution requires IEEE permission.
See http://www.ieee.org/publications_standards/publications/rights/index.html for more information.

Authorized licensed use limited to: Nanyang Technological University Library. Downloaded on November 14,2024 at 14:27:51 UTC from IEEE Xplore. Restrictions apply.

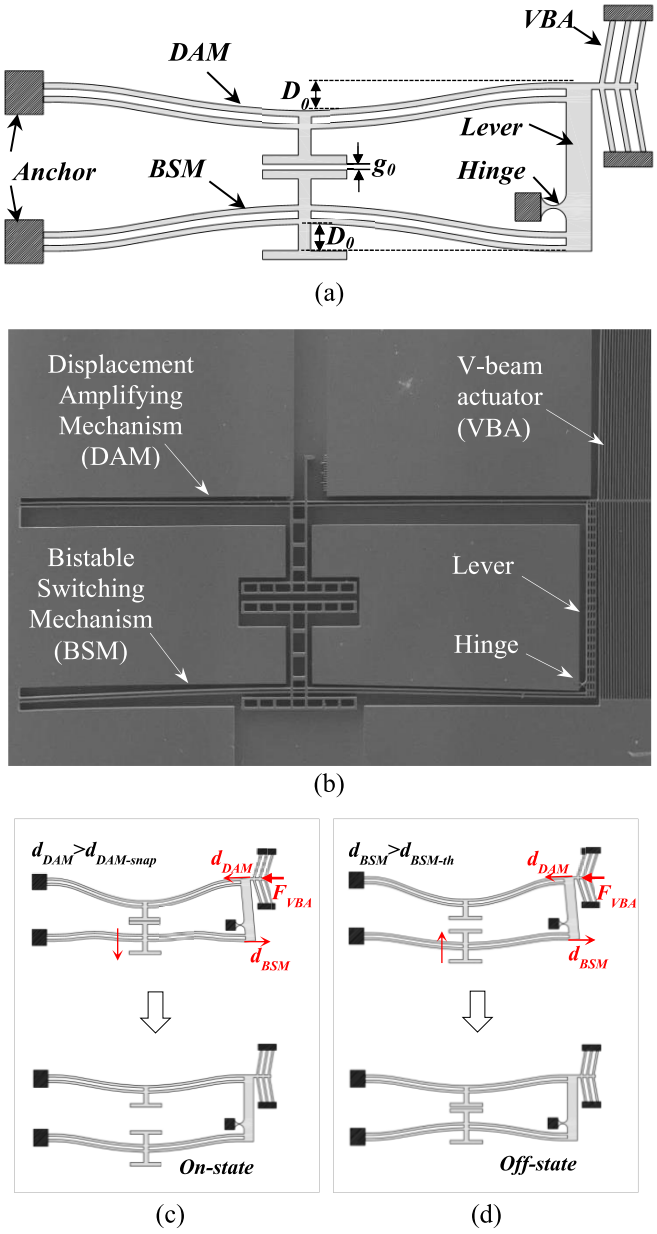

Fig. 1. (a) Schematics of the MEMS Push-On-Push-Off bistable device. (b) The SEM picture of the push-on push-off bistable device. (c) Sequence of the push-on action. (d) Sequence of the push-off action.

to switch from the *Off-state* to the *On-state* (i.e., snap-through occurs.). Further discussion on $d_{DAM-push-on}$ is presented in Section IIIB.

The push-off transition is shown in Fig. 1(d). When a DC voltage is applied to the VBA, the BSM end displacement (d_{BSM}) is generated. As d_{BSM} exceeds a threshold value $d_{BSM-vanish}$, the bistability of the BSM vanishes, and the BSM is released (snapped through) from the On-state to the Off-state. A brief derivation of $d_{BSM-vanish}$ is provided in Appendix A.

Fig. 2 shows schematics of the equivalent model used for studying the device operation. As shown in Fig. 2(a), when the VBA is actuated, it generates an end displacement d_{DAM} in the axial direction of the DAM. This end displacement produces a relatively large transverse displacement (D_{DAM}) at the central

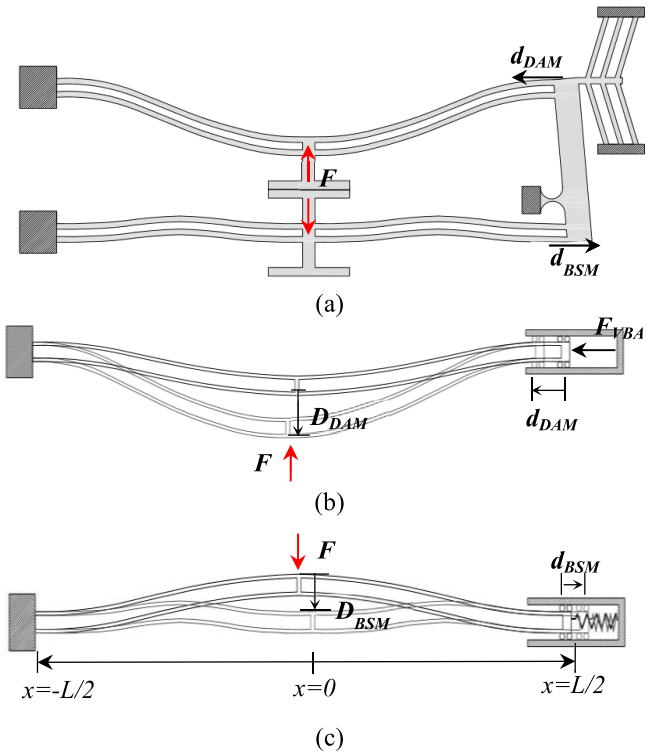

Fig. 2. (a) Schematic of the Push-On-Push-Off system, (b) the corresponding models of the DAM and (c) the BSM.

point of the curved-beam of the DAM. Subsequently, the DAM touches and pushes the BSM with force F. Figs. 2(b) and 2(c) show schematics corresponding to the DAM and BSM.

As shown in Fig. 2(b), one of the two ends of the DAM is clamped to a wall, whereas the other end is free to move in the axial direction. The double-curved beam is subjected to an axial force F_{VBA} applied by the VBA, and this force causes an end displacement d_{DAM}. The DAM is subjected to a transverse force F at the central point when it is in contact with the BSM.

Fig. 2(c) shows a schematic of an equivalent model of BSM similar to that of DAM. The BSM can be considered as a double-curved beam, with one end clamped to a wall and the other end supported by a spring with stiffness k_{BSM}. The end displacement d_{BSM} is designed to be proportional to d_{DAM} with a factor η which is defined by the dimensions of the lever. Detailed discussions on η will be given in Section III.A. Notably, we have $d_{BSM} > 0$ if the BSM's end is stretched. The transverse force F applied to the midpoint of the DAM and BSM is a counterforce. We assume that both the curved beams and the end springs are initially in the unstrained state.

Fig. 3 shows the force–displacement curves for the DAM and BSM. The transverse displacements of the DAM and BSM are denoted by D_{DAM} and D_{BSM}. The slope of the curves indicates the transverse stiffness (i.e., the stiffness in the transverse direction). Each force–displacement curve has three regions of different stiffness. Two regions of very large positive stiffness constants are around the beginning and the end of the curve. Also, a region of low negative stiffness is located in between. Assume that the dimensions of the curved beams of both the DAM and BSM are identical.

Authorized licensed use limited to: Nanyang Technological University Library. Downloaded on November 14,2024 at 14:27:51 UTC from IEEE Xplore. Restrictions apply.

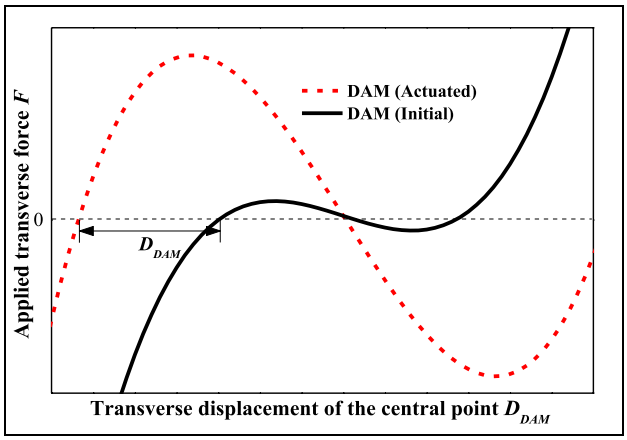

(a)

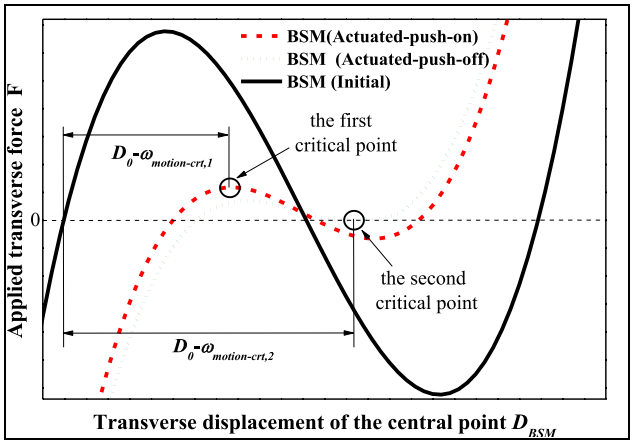

(b)

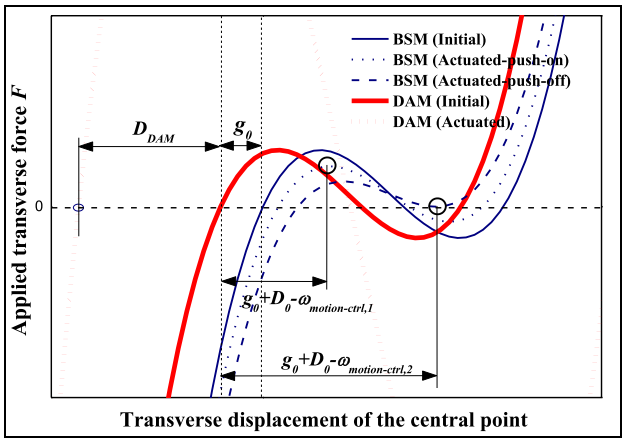

(c)

Fig. 3. Curved beams' transverse displacements versus applied forces: (a) DAM, (b) BSM, and (c) combined relationship of the DAM the BSM.

The solid curves then represent the force–displacement relationships of the DAM and BSM without end displacements (i.e., $d_{BSM} = 0$ and $d_{DAM} = 0$).

As shown in Fig. 3(a), when end displacements are generated at the end of the DAM, the local maximum and local minimum of the curve increase, reflecting an increase in the stiffness for the transverse motion of the DAM. Furthermore, the lever pulls the end of the BSM as the end of the DAM is pushed. Consequently, the "stiffness" for the transverse motion of the BSM decreases, and the local minimum and the local maximum of the BSM curve decrease. In Fig. 3(b), the dashed line is the curve after the BSM snaps through to On-state, and the dotted line is the force–displacement curve at the condition when the bistability of the BSM vanishes. Fig. 3(c) shows the combined relationship of the DAM the BSM.

The main functionality of the DAM is to generate a sufficiently large transverse displacement (D_{DAM}) to push the BSM to snap through to the On-state. To push the BSM from the Off-state to the On-state, the DAM should push the BSM over its first critical point, as shown in Fig. 3(b). Therefore, when the device snaps from the Off-state to the On-state, the following condition must be satisfied:

$$D_{DAM} > g_0 + D_0 - \omega_{motion-crt,1} = D_{DAM-push-on} \quad (1)$$

where $D_{DAM-push-on}$ is the required minimum value of the DAM's transverse displacement that will make D_{DAM} sufficiently large to push the BSM to switch from the Off-state to the On-state, g_0 is the initial gap between the DAM and the BSM, D_0 is the initial central offset of both the DAM and BSM, and $\omega_{motion-crt,1}$ is the central offset of the BSM as the structure snaps from the Off-state to the On-state. The derivation of the closed form of $\omega_{motion-crt,1}$ is presented in Appendix A.

The push-off process is also actuated by the DAM. Therefore, it is essential to ensure that D_{DAM} is not so large that it blocks the BSM from snapping back to the Off-state during the push-off process. In other words, the total transverse displacement of the DAM should not exceed the second critical point (shown in Fig. 3(b)), and the following condition should be satisfied:

$$D_{DAM} < g_0 + D_0 - \omega_{motion-crt,2} = D_{DAM-max} \quad (2)$$

where $D_{DAM-max}$ is the maximum value of the DAM's transverse displacement that will not prevent the BSM from being released from the On-state to Off-state, and $\omega_{motion-crt,2}$ is the central offset of the BSM as the BSM snaps from the On-state to the Off-state. The derivation of $\omega_{motion-crt,2}$ is presented in Appendix A.

III. Design Criteria

In this section, we derive and discuss the criteria that can be used to ensure the bistability and push-on push-off capability.

A. Bistability

The bistability of a typical BSM structure with fixed boundary conditions on both ends has been extensively discussed in [16]. In the this study, however, one of the two ends of the BSM is connected to a lever (i.e., a non-rigid boundary, as shown in Fig. 1(a)). As shown in Fig. 2(c), this non-rigid boundary can be considered as a linear spring oriented along the axial direction. The stiffness of this conceptual spring (k_{BSM}) should be sufficiently large to ensure the bistability of the BSM, so that the device can stably stay in either of the two stable positions.

The governing equation of the BSM can be written as:

$$EI \cdot (y^{(4)} - y_0^{(4)}) + P \cdot y^{(2)} = -F \cdot \delta(x) \quad (3)$$

Authorized licensed use limited to: Nanyang Technological University Library. Downloaded on November 14,2024 at 14:27:51 UTC from IEEE Xplore. Restrictions apply.

where $y_0(x)$ is the initial shape of the curve beam with the two ends being separated by a distance L, $y(x)$ is the shape of the curve beam after being stretched or compressed, F is the transverse force loading at the midpoint, and $\delta(x)$ is the impulse function. The parameters E and I denote Young's modulus and the area moment of the inertia of the cross section of the curved beam, respectively.

According to Hooke's law, the axial force by the conceptual spring is

$$P = k_{BSM} \cdot \delta_{BSM}. \tag{4}$$

where δ_{BSM} is the deformation of the conceptual spring in axial direction from the BSM initial position, and can be related to the deformed shape $y(x)$ by considering the equilibrium of the end of the curved beam:

$$\delta_{BSM} = -\frac{PL}{EA} + \frac{1}{2}\int_{L/2}^{-L/2} \left(\left(y_0'\right)^2 - \left(y'\right)^2\right) dx. \tag{5}$$

where A is the cross-sectional area of the curved beam. The first term on the right-hand side represents the axial deformation caused by the axial force, and the second term represents the foreshortening effect of the laterally deformed shape.

Combining (4) and (5) and eliminating δ_{BSM}, the axial force P can be written as

$$P = \kappa \cdot \frac{EA}{2L}\int_{L/2}^{L/2} \left(\left(y_0'\right)^2 - \left(y'\right)^2\right) dx \tag{6}$$

where κ is the nondimensional spring stiffness

$$\kappa = \frac{k_{BSM}L}{k_{BSM}L + EA} \quad 0 \le \kappa \le 1 \tag{7}$$

The boundary conditions are

$$\begin{aligned} y_0(L/2) = y_0(-L/2) = y_0'(L/2) = y_0'(-L/2) = 0 \\ y(L/2) = y(-L/2) = y'(L/2) = y'(-L/2) = 0. \end{aligned} \tag{8}$$

The initial (as-fabricated) shape of the unstrained BSM is

$$y_0(x) = \frac{D_0}{2}(1 + \cos(\gamma x)) \tag{9}$$

where $\gamma = 2\pi/L$. In addition, the shape of the BSM after being stretched or compressed can be expressed as a linear combination of mode shape functions $(1 + \cos(n\gamma x))/2$:

$$y(x) = \sum_{n=1,3,5,odd}^{\infty} \omega_n \frac{(1 + \cos(n\gamma x))}{2} \tag{10}$$

where ω_n is the coefficient of each mode shape function.

For deriving the criterion analytically, we approximate the BSM shape by using the first mode shape function [16], [19]:

$$y(x) = \frac{\omega_1}{2}(1 + \cos(\gamma x)) \tag{11}$$

Substituting (9) and (11) into (6), we obtain

$$P = \frac{EA\kappa\gamma^2}{16}(D_0^2 - \omega_1^2). \tag{12}$$

Using the Galerkin method [19], [20], we substitute (9), (11), and (12) in (3). Further, both sides of the equation are multiplied by $\cos(\gamma x)$ and integrated from $x = -L/2$ to $L/2$ by employing the orthonormality of the eigenfunctions. Thus, we obtain

$$F = \frac{-\gamma^4 LEA}{64}\left(\kappa \cdot \omega_1^3 - \alpha \cdot \omega_1 - \beta\right) \tag{13}$$

where $\alpha = -\left(\frac{16I}{A} - \kappa D_0^2\right)$ and $\beta = \frac{16ID_0}{A}$.

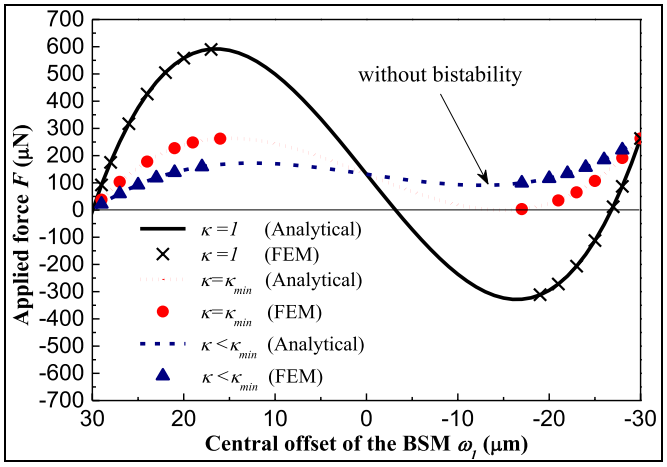

Fig. 4. Relationship of the applied force versus the transverse displacement of the BSM ($L = 4000\mu$m). The points marked by crosses are the simulated results by the Coventorware.

Fig. 4 shows the curves of F vs. ω_1. The local maximum and local minimum of these curves are the critical points when snap-through occurs. The parameters F and ω_1 at these points are the critical forces and critical positions, respectively. By setting the derivative of (13) to be zero, we obtain

$$\frac{dF}{d\omega_1} = \frac{-\gamma^4 LEA}{64}(3\kappa\omega_1^2 - \alpha) = 0. \tag{14}$$

Then, we obtain the critical positions

$$\omega_{spring-crt,1} = \sqrt{\frac{\alpha}{3\kappa}} \tag{15}$$

$$\omega_{spring-crt,2} = -\sqrt{\frac{\alpha}{3\kappa}}. \tag{16}$$

The critical forces can be obtained by substituting these critical positions into (13):

$$F_{spring-crt,1} = \frac{EAL\gamma^4}{64}\left(\frac{2}{3\sqrt{3\kappa}}\alpha^{3/2} + \beta\right) \tag{17}$$

$$F_{spring-crt,2} = \frac{-EAL\gamma^4}{64}\left(\frac{2}{3\sqrt{3\kappa}}\alpha^{3/2} - \beta\right). \tag{18}$$

As shown in Fig. 4, when the local minimum ($F_{spring-crt,2}$) of the curves exceeds zero, the BSM cannot stably stay in the On-state. In other words, the BSM will return to the Off-state when the external force is removed. In this situation, the BSM is not bistable. Therefore, the condition for the bistability of the BSM can be derived by setting $F_{spring-crt,2} = 0$:

$$\left(\frac{2}{3\sqrt{3\kappa}}\alpha^{3/2} - \beta\right) = 0. \tag{19}$$

Authorized licensed use limited to: Nanyang Technological University Library. Downloaded on November 14,2024 at 14:27:51 UTC from IEEE Xplore. Restrictions apply.

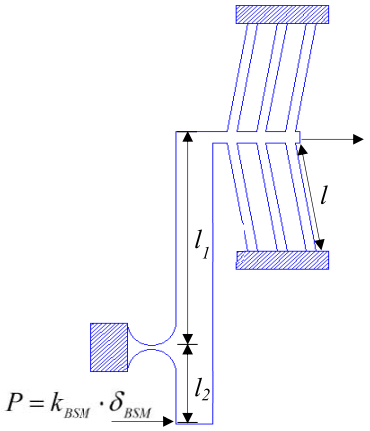

Fig. 5. Schematic of the end spring of the BSM.

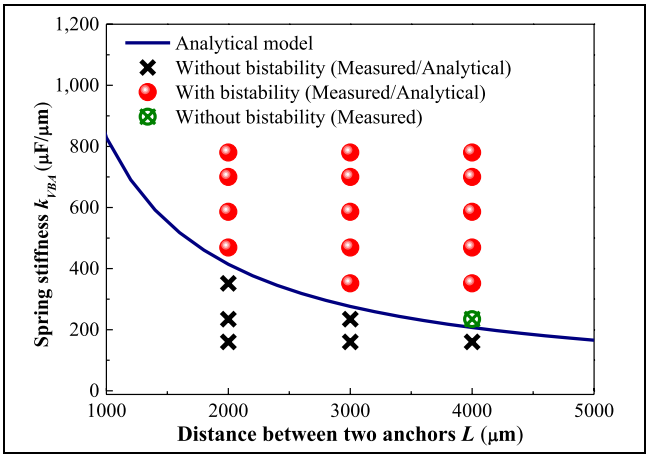

Fig. 6. Critical curve for $\zeta = 1$ from theoretical solution to determine whether the bistable behavior occurs or not. The dots and crosses are experimental results.

Then, the corresponding minimum nondimensional spring stiffness κ_{min} for sustaining the bistability of the curved beam can be expressed as

$$\kappa_{min} = \frac{64I}{AD_0^2}. \tag{20}$$

Substituting (20) into (7), we obtain the minimum spring stiffness required to sustain the BSM bistability of the curved beam:

$$k_{min} = \frac{EA}{L}\left(\frac{AD_0^2}{64I} - 1\right)^{-1} \tag{21}$$

Because the BSM is actually a double-curved-beam structure, the minimum required stiffness of the conceptual spring k_{BSM} to sustain the BSM bistability should be twice of k_{min}:

$$k_{BSM-min} = 2 \cdot k_{min} \tag{22}$$

The end spring constant k_{BSM} is actually the total equivalent spring constant of a structure consisting of the VBA, the lever, and a flexure hinge, as shown in Fig. 5. It is well known that the VBA has a very stiff structure. Therefore, the stiffness of the hinge is considered to be negligible. Moreover, the lever is assumed to be a rigid body. The analytical form of the VBA spring stiffness (k_{VBA}) can be found in [21]:

$$k_{VBA} = N \cdot \frac{24EI_V \cos^2\theta + 2EA_V l^2 \sin^2\theta}{l^3} \tag{23}$$

where N is the number of V-beam, θ is the inclined angle, l is half the length of the V-beam, I_V is the moment of inertia of the V-beam, and A_V is the cross-sectional area of the V-beam.

The balance of the torque around the hinge of the lever gives

$$P_{VBA} \cdot l_1 = P \cdot l_2 \tag{24}$$

where $P_{VBA} = k_{VBA} \cdot \delta_{DAM}$, $P = k_{BSM} \cdot \delta_{BSM}$, l_1 is the length of the long arm of the lever, and l_2 is the length of the short arm of the lever. Therefore, We can write (24) as a relationship between k_{VBA} and $k_{BSM-\min}$:

$$k_{VBA} \cdot \delta_{DAM} \cdot l_1 = k_{BSM} \cdot \delta_{BSM} \cdot l_2. \tag{25}$$

Here we define the lever ratio as $\eta = l_1/l_2$. Therefore, $\delta_{DAM}/\delta_{BSM} = \eta$, and (25) can be rewritten as

$$k_{BSM} = \eta^2 \cdot k_{VBA}. \tag{26}$$

In addition, to ensure bistability, the axial stiffness k_{BSM} should be larger than the minimum axial stiffness $k_{BSM-min}$:

$$k_{BSM} > k_{BSM-min}. \tag{27}$$

Therefore, combining (26) and (27), we obtain the criterion for the existence of bistability:

$$\zeta = \frac{\eta^2 \cdot k_{VBA}}{k_{BSM-min}} > 1 \tag{28}$$

where ζ is a nondimensional stiffness ratio. This ratio is proposed as an index for determining the existence of bistability.

Fig. 6 presents experimentally and theoretically obtained plots of k_{VBA} vs. beam length L. The figure also shows the curve for $\zeta = 1$, which was obtained using (22) and (28). According to (28), the device is bistable when $\zeta > 1$, which is actually the region above the curve of $\zeta = 1$ in Fig. 6. The region below the curve is the region ($\zeta < 1$) in which bistability does not exist. The circles and crosses in Fig. 6 denote measured results of devices with different values of L and k_{VBA}. For each device, k_{VBA} was calculated based on (23). The dimensions of components considered in the experiment are presented in Table I. The circles denote devices that are bistable, and the crosses indicate devices that do not show bistability. The measurement results are in favorable agreement with the theoretical prediction presented in this section.

B. Push-On Push-Off Capability

As mentioned, both the push-on and push-off processes are actuated by the VBA. For the push-on process, the VBA actuates the DAM and then pushes the BSM to the On-state. For the push-off process, the VBA pulls the end of the BSM through the lever until the bistability of the BSM disappears, resulting in the BSM snapping to the Off-state. To ensure that a device has both push-on and push-off capabilities, two conditions must be satisfied.

Authorized licensed use limited to: Nanyang Technological University Library. Downloaded on November 14,2024 at 14:27:51 UTC from IEEE Xplore. Restrictions apply.

TABLE I
DIMENSIONS AND MATERIAL PROPERTIES OF TESTED DEVICES

Curved beam length (L)	2000, 3000, 4000 μm
Young's modules (E)	169 GPa
Length of the lever (l_1+l_2)	1500 μm
Width of the curved beam (w)	8 μm
Initial Central Offset (D_0)	30 μm
Half V-beam length (l)	500 μm
Cross area of the V-beam(A_v)	1000 μm^2
Inclined angle of the V-beam (θ)	1°
Cross area of the curved beam(A)	800 μm^2

1. *Push-On Process:* Because the BSM should retain its bistability during the push-on process, the end displacement of the BSM for achieving push on ($d_{BSM-push-on}$) should be less than a threshold value ($d_{BSM-vanish}$), which eliminates the bistability of the BSM:

$$d_{BSM-push-on} < d_{BSM-vanish} \tag{29}$$

Note that the derivation of $d_{BSM-vanish}$ is provided in Appendix A.

2. *Push-Off Process:* During the push-off process, it is necessary that $d_{DAM-push-off}$ is not so large that it generates a transverse displacement D_{DAM} that blocks the BSM from snapping to the Off-state. Therefore, we obtain

$$d_{DAM-push-off} < d_{DAM-max}. \tag{30}$$

Note that $d_{DAM-max}$ can be evaluated from $D_{DAM-max}$ (shown in (2)) by using the analytical formula provided in Appendix B [22].

In addition, on the basis of the lever principle, we obtain the following relationships:

$$\begin{aligned} d_{BSM-push-on} &= d_{DAM-push-on}/\eta \\ d_{DAM-push-off} &= d_{BSM-vanish} \cdot \eta. \end{aligned} \tag{31}$$

Combining (29), (30), and (31), we obtain the criterion for the push-on push-off capability:

$$\frac{d_{DAM-push-on}}{d_{BSM-vanish}} < \eta < \frac{d_{DAM-max}}{d_{BSM-vanish}}. \tag{32}$$

The parameter $d_{DAM-push-on}$ can be calculated from $D_{DAM-push-on}$ (shown in (1)) by using the closed-form relationship provided in Appendix B.

Fig. 7 shows plots of the actuator output (d_{DAM}) against η, and it can be used to describe the criterion for the push-on push-off capability. In Fig. 7, there are three major curves which are described as follows:

1. The solid line is calculated from the expression $d_{DAM} = \eta \cdot d_{BSM-vanish}$. In the region above this line, the bistability of the BSM vanishes because d_{DAM} is so large that d_{BSM} exceeds $d_{BSM-vanish}$. Therefore, the push-off action, which is achieved by eliminating the bistability of the BSM, requires d_{DAM} to be above this line.
2. The dashed line is a plot of $d_{DAM} = d_{DAM-push-on}$ vs. η. In the region below this curve, the push-on action cannot be achieved because d_{DAM} is insufficient to push

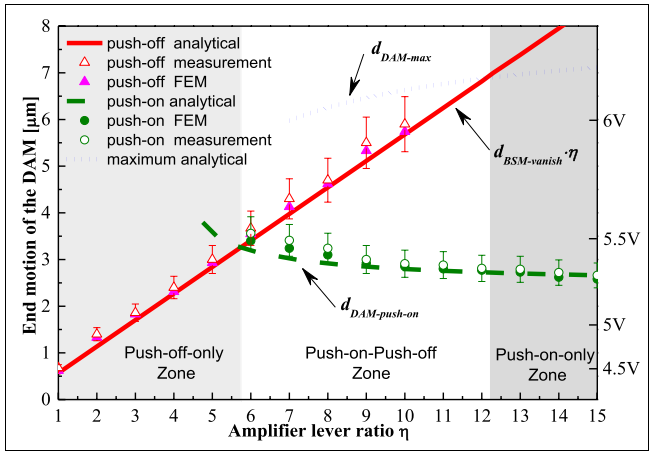

(a)

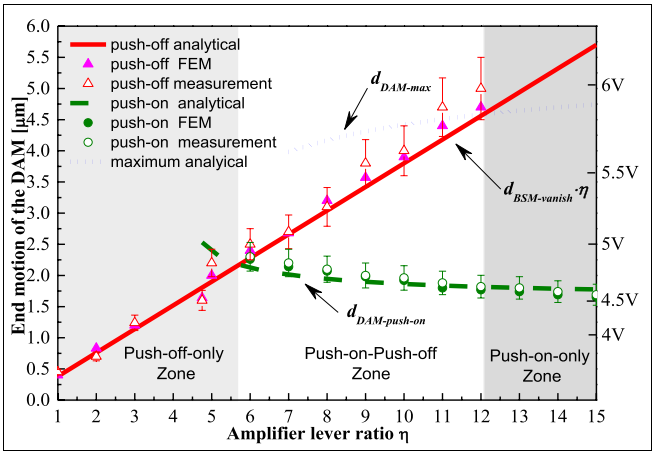

(b)

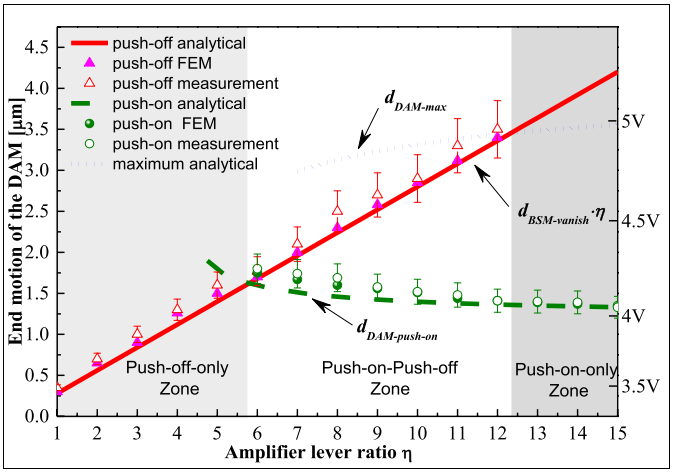

(c)

Fig. 7. The amplifier lever ratio versus the end motion of the DAM for Push-On and Push-Off for the devices with different curved beam length (a) 2000 μm (b) 3000 μm (c) 4000 μm. The corresponding actuation voltages are also indicated in the figures.

Authorized licensed use limited to: Nanyang Technological University Library. Downloaded on November 14,2024 at 14:27:51 UTC from IEEE Xplore. Restrictions apply.

TABLE II
CALCULATED RESULTS OF PUSH-ON-PUSH-OFF PARAMETERS

L	2000 μm	3000 μm	4000 μm
η	$5.7<\eta<12.2$	$5.7<\eta<12.2$	$5.7<\eta<12.4$

the BSM to the On-state. Therefore, the push-on action requires d_{DAM} to be above this line.

3. The dotted line is the maximum allowable d_{DAM} for achieving push-off action (i.e., $d_{DAM} = d_{DAM-max}$ vs. η). In the region above this line, the DAM blocks the BSM from returning to the Off-state.

The intersection point of the curves $d_{DAM} = d_{DAM-push-on}$ vs. η and $d_{DAM} = \eta \cdot d_{BSM-vanish}$ vs. η is the lower limit of the push-on push-off capability. By contrast, the intersection point of the curves $d_{DAM} = d_{DAM-max}$ vs. η and $d_{DAM} = \eta \cdot d_{BSM-vanish}$ vs. η is the upper limit of the push-on push-off capability.

As shown in Fig. 7, the lever ratio η at these two intersection points can be used to divide this figure into three zones: the "push-off-only" zone, the "push-on push-off" zone, and the "push-on-only" zone. In the "push-off-only" zone, η is below the lower boundary of (32), and therefore, the device cannot achieve push-on action because the bistability of the BSM disappears before snap-through occurs. In the push-on-only region, the push-off action cannot be achieved because d_{DAM} is so large that the DAM blocks the BSM from returning to the Off-state during the push-off action (i.e., $d_{DAM} = \eta \cdot d_{BSM-vanish} \geq d_{DAM-max}$). Finally, the "push-on push-off" region satisfies the condition of (32). Notably, the range of d_{DAM} in the push-on push-off region increases with η. Table II lists the calculated intersection points for different device lengths (L) by using the analytical formulas presented in this section.

Measurement results are also shown in Fig. 7. Over 100 devices with different dimensions were tested. For each data point in the figure, the values of d_{DAM} were transformed using applied voltages based on the thermomechanical modeling in [23]. The test results were in reasonably good agreement with the analytical predictions. In summary, the modeled and measurement results described in this section indicate that the device designs satisfied with the condition of (32) possess the push-on push-off capability.

IV. CONCLUSION

In this study, design criteria for a MEMS push-on push-off bistable device are presented. The first design criterion provides conditions that can be used for determining the device bistability, and the second design criterion presents conditions that can be used to examine the existence of the push-on push-off capability. Both criteria are expected to be useful for designers for rapidly designing bistable devices with push-on push-off capability. The criteria were derived in closed forms. The criterion that determines the device bistability is represented in terms of a spring stiffness ratio, and the criterion that measures the push-on push-off capability is represented in terms of a lever ratio. Experimental results by measuring more than 100 devices with different dimensions validated the analytical derivations for both criteria.

APPENDIX

A. End Displacement Analysis of BSM

Here, we derive the analytical form of the required BSM end displacement d_{BSM} to eliminate the bistability of the BSM. According to (5), the axial force of the BSM for a prescribed end displacement is

$$P = -\frac{EAd_{BSM}}{L} + \frac{EA}{2L}\int_{-L/2}^{L/2}\left((y_0')^2 - (y')^2\right)dx. \quad \text{(A1)}$$

Following steps similar to those described in Section III-A, we obtain

$$F = -\frac{EAL\gamma^4}{64}\left(\omega_1^3 - \alpha_1 \cdot \omega_1 - \beta_1\right) \quad \text{(A2)}$$

where

$$\alpha_1 = -\left(\frac{16I}{A} + \frac{16d_{BSM}}{L\gamma^2} - D_0^2\right), \quad \beta_1 = \frac{16ID_0}{A}.$$

By setting the derivative of (A2) to be zero, we obtain the critical positions:

$$\omega_{motion-crt,1} = \sqrt{\frac{\alpha_1}{3}} \quad \text{(A3)}$$

$$\omega_{motion-crt,2} = -\sqrt{\frac{\alpha_1}{3}}. \quad \text{(A4)}$$

The corresponding critical loads can be obtained by substituting (A3) and (A4) in (A2):

$$F_{motion-crt,1} = \frac{EAL\gamma^4}{64}\left(\frac{2}{3\sqrt{3}}\alpha_1^{3/2} + \beta_1\right) \quad \text{(A5)}$$

$$F_{motion-crt,2} = -\frac{EAL\gamma^4}{64}\left(\frac{2}{3\sqrt{3}}\alpha_1^{3/2} - \beta_1\right) \quad \text{(A6)}$$

The critical condition required for determining the existence of the BSM bistability can be derived by setting $F_{motion-crt,2} = 0$:

$$\left(\frac{2}{3\sqrt{3}}\alpha_1^{3/2} - \beta_1\right) = 0. \quad \text{(A7)}$$

Therefore, the required BSM end displacement d_{BSM} to eliminate the bistability of the BSM is:

$$d_{BSM-vanish} = \frac{\pi^2}{4L}\left(D_0^2 - \frac{4}{3}w^2 - \sqrt[3]{12 \cdot w^4 \cdot D_0^2}\right) \quad \text{(A8)}$$

B. End Displacement vs. Transverse Displacement for a Curved Beam

As shown in Fig. 2(b), d_{DAM} generates D_{DAM}. According to a study by Saif and MacDonald [22], the relationship between d_{DAM} and D_{DAM} for zero transverse load ($F = 0$) is

$$d_{DAM} = \frac{\pi^2}{4L}\left[(D_{DAM} + D_0)^2 - D_0^2\right] \quad \text{(A9)}$$

where D_0 is the initial central offset of the curved beam.

Fig. 8 presents the curves of (A9). The figure also shows the FEM simulated results (by using Coventorware). The results validate the analytical model.

Authorized licensed use limited to: Nanyang Technological University Library. Downloaded on November 14,2024 at 14:27:51 UTC from IEEE Xplore. Restrictions apply.

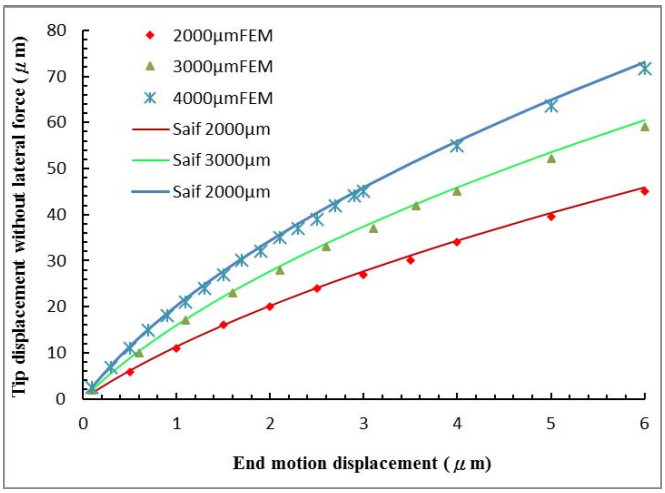

Fig. 8. The end displacement vs. the transverse displacement of the DAM without a transverse load.

C. Nomenclature

A	Cross-sectional area of the curved beam.
A_V	Cross-sectional area of a V-beam.
D_0	Initial central offset of a curved beam.
D_{BSM}	Transverse displacement of the BSM.
D_{DAM}	Transverse displacement of the DAM.
$D_{DAM-push-on}$	Transverse displacement of the DAM for achieving push-on.
$D_{DAM-max}$	Maximum value of the DAM transverse displacement without blocking the BSM from snapping back to the Off-state.
d_{BSM}	End displacement of the BSM.
d_{DAM}	End displacement of the DAM.
$d_{BSM-push-on}$	End displacement of the BSM for achieving push-on.
$d_{DAM-push-on}$	End displacement of the DAM for achieving push-on.
$d_{BSM-vanish}$	Minimum BSM end displacement for eliminating the bistability of the BSM.
$d_{DAM-push-off}$	DAM end displacement for achieving push-off
$d_{DAM-max}$	Maximum value of the DAM end displacement that will not block the BSM from snapping back to the Off-state.
E	Young's modulus of silicon.
F	Transverse force on the mid-point of the curved beam.
$F_{spring-crt,1}$	First critical transverse force of the BSM when unactuated.
$F_{spring-crt,2}$	Second critical transverse force of the BSM when unactuated.
F_{VBA}	VBA actuating force applied on the end of the DAM.
$F_{motion-crt,1}$	First critical transverse force of the BSM when actuated.
$F_{motion-crt,2}$	Second critical transverse force of the BSM when actuated.
g_0	Initial gap between the contact points of the DAM and the BSM.
I	Curved beam moment of the inertia.
I_V	moment of the inertia of a V-beam.
k_{BSM}	Stiffness of the conceptual spring connected to the end of the BSM.
k_{VBA}	Stiffness of the VBA in axial direction.
$k_{BSM-min}$	Minimum spring stiffness for sustaining the bistability of the BSM.
L	Distance between the two anchors of a curved beam.
l	Half length of a V-beam.
N	Number of V-beams in the VBA.
P	Axial force of the BSM.
P_{VBA}	Axial force of the DAM when unactuated.
$y_0(x)$	Initial shape function of the BSM.
$y(x)$	Shape function of BSM after being stretched or compressed.
$\delta(x)$	Dirac delta function.
δ_{BSM}	Deformation of the conceptual spring connected to the end of the BSM.
δ_{DAM}	Deformation of DAM induced by δ_{BSM}, and $\delta_{DAM} = \delta_{BSM} \cdot \eta$
η	Level ratio: $\eta = l_1/l_2$, where l_1 is the length of the long arm, and l_2 is the length of the short arm.
κ	Nondimensional spring stiffness.
κ_{min}	Minimum nondimensional spring stiffness.
θ	Inclined angle of the VBA.
$\omega_{spring-crt,1}$	BSM central offset of the first critical point when unactuated.
$\omega_{spring-crt,2}$	The BSM's central offset of the second critical point when unactuated.
$\omega_{motion-crt,1}$	BSM central offset of the first critical point when actuated.
$\omega_{motion-crt,2}$	BSM central offset of the second critical point when actuated.

ACKNOWLEDGMENT

The authors are grateful to Mr. Fan-Chi Lin's help with the measurements.

REFERENCES

[1] B. Ando, S. Baglio, G. L'Episcopo, and C. Trigona, "Investigation on mechanically bistable MEMS devices for energy harvesting from vibrations," *J. Microelectromech. Syst.*, vol. 21, no. 4, pp. 779–790, 2012.

[2] M. Sulfridge, T. Saif, N. Miller, and K. O'Hara, "Optical actuation of a bistable MEMS," *J. Microelectromech. Syst.*, vol. 11, no. 5, pp. 574–583, 2002.

[3] H. Matoba, T. Ishikawa, C.-J. Kim, and R. S. Muller, "A bistable snapping microactuator," in *Proc. IEEE MEMS*, Oiso, Japan, 1994, pp. 45–50.

[4] Y. Gerson, S. Krylov, and B. Ilic, "Electrothermal bistability tuning in a large displacement micro actuator," *J. Micromech. Microeng.*, vol. 20, no. 11, p. 112001, 2010.

[5] Y. Wu, C. Zhang, H. Wang, and G. Ding, "Torsion/cantilever-based MEMS bistable mechanisms with different support configurations: Structure design and comparison," *J. Micromech. Microeng.*, vol. 21, no. 4, p. 045007, 2011.

[6] B. Charlot, W. Sun, K. Yamashita, H. Fujita, and H. Toshiyoshi, "Bistable nanowire for micromechanical memory," *J. Micromech. Microeng.*, vol. 18, no. 4, p. 045005, 2008.

Authorized licensed use limited to: Nanyang Technological University Library. Downloaded on November 14,2024 at 14:27:51 UTC from IEEE Xplore. Restrictions apply.

[7] S. Krylov, B. R. Ilic, D. Schreiber, S. Seretensky, and H. Craighead, "The pull-in behavior of electrostatically actuated bistable microstructures," *J. Micromech. Microeng.*, vol. 18, no. 5, p. 055026, 2008.
[8] J. Qiu, J. H. Lang, A. H. Slocum, and A. C. Weber, "A bulk-micromachined bistable relay with U-shaped thermal actuators," *J. Microelectromech. Syst.*, vol. 14, no. 5, pp. 1099–1109, Oct. 2005.
[9] T. Gomm, L. L. Howell, and R. H. Selfridge, "In-plane linear displacement bistable microrelay," *J. Micromech. Microeng.*, vol. 12, no. 3, pp. 257–264, 2005.
[10] J. Barth, C. Megnin, and M. Kohl, "A bistable shape memory alloy microvalve with magnetostatic latches," *J. Microelectromech. Syst.*, vol. 21, no. 1, pp. 76–84, 2012.
[11] R. Luharuka and P. J. Hesketh, "A bistable electromagnetically actuated rotary gate microvalve," *J. Micromech. Microeng.*, vol. 18, no. 3, p. 035015, 2008.
[12] Y.-J. Yang, B.-T. Liao, and W.-C. Kuo, "A novel 2 × 2 MEMS optical switch using the split cross-bar design," *J. Micromech. Microeng.*, vol. 17, no. 5, pp. 875–882, 2007.
[13] I.-H. Hwang, Y.-S. Shim, and J.-H. Lee, "Modeling and experimental characterization of the chevron-type bi-stable microactuator," *J. Micromech. Microeng.*, vol. 13, no. 6, pp. 948–954, 2003.
[14] R. A. M. Receveur, C. R. Marxer, R. Woering, V. C. M. H. Larik, and N.-F. de Rooij, "Laterally moving bistable MEMS DC switch for biomedical applications," *J. Microelectromech. Syst.*, vol. 14, no. 5, pp. 1089–1098, 2005.
[15] H.-W. Huang and Y.-J. Yang, "A MEMS bistable device with push-on–push-off capability," *J. Microelectromech. Syst.*, vol. 22, no. 1, pp. 7–9, 2013.
[16] J. Qiu, J. H. Lang, and A. H. Slocum, "A curved-beam bistable mechanism," *J. Microelectromech. Syst.*, vol. 13, no. 2, pp. 137–146, Apr. 2004.
[17] C. Lee and C.-Y. Wu, "Study of electrothermal V-beam actuators and latched mechanism for optical switch," *J. Micromech. Microeng.*, vol. 15, no. 1, p. 11, 2005.
[18] F. Marty *et al.*, "Advanced etching of silicon based on deep reactive ion etching for silicon high aspect ratio microstructures and three-dimensional micro- and nanostructures," *Microelectron. J.*, vol. 36, no. 7, pp. 673–677, 2005.
[19] M. T. A. Saif, "On a tunable bistable MEMS-theory and experiment," *J. Microelectromech. Syst.*, vol. 9, no. 2, pp. 157–170, 2000.
[20] S. D. Senturia, *Microsystem Design*, Boston, MA, USA: Kluwer, 2001, pp. 231–235.
[21] Y. Zhu, A. Corigliano, and H. D. Espinosa, "A thermal actuator for nanoscale *in situ* microscopy testing: Design and characterization," *J. Micromech. Microeng.*, vol. 16, no. 2, pp. 242–253, 2006.
[22] M. T. A. Saif and N. C. MacDonald, "A millinewton microloading device," *Sens. Actuators A, Phys.*, vol. 52, pp. 65–75, Mar./Apr. 1996.
[23] E. T. Enikov, S. S. Kedar, and K. V. Lazarov, "Analytical model for analysis and design of V-shaped thermal microactuators," *J. Microelectromech. Syst.*, vol. 14, pp. 788–798, 2005.

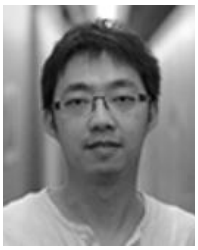

Hen-Wei Huang (S'15) received the bachelor's and master's degrees in mechanical engineering from National Taiwan University (NTU) in 2011 and 2012, respectively, with a minor in chemical engineering and geography during the period of bachelor's degree. He is currently pursuing the Ph.D. degree with the Multi-Scale Robotics Laboratory, Swiss Federal Institute of Technology. After one year military service, he worked as a Research Assistant with the Applied Science Center, Academic Sinica, and the Graduate Institute of Electronics Engineering, NTU.

His research interests include wireless sensor network, embedded systems for biomedical applications, bi-stable microactuators, sensor technologies, microfluidics, and lab on chips. He is a member of ASME, CSME, and STAM. He is also a recipient of the Outstanding Creativity Performance Scholarship of the CTCI Foundation and the MOE Technologies Incubation Scholarship.

Fu-Wei Lee received the B.S. degree from the Department of Mechanical Engineering, National Taiwan University, Taiwan, in 2014, where he is currently pursuing the M.S. degree with the Department of Mechanical Engineering. His research interests include bi-stable microactuators and micromachining techniques.

Yao-Joe Joseph Yang (S'98–M'01) received the B.S. and M.S. degrees in mechanical engineering from National Taiwan University in 1990 and 1995, respectively, and the M.S. and Ph.D. degrees in electrical engineering from the Massachusetts Institute of Technology in 1997 and 1999, respectively.

He joined as a Senior Application Engineer the Coventor, Inc., Cambridge, MA, from 1999 to 2000. Since 2000, he has been with the Department of Mechanical Engineering, National Taiwan University, where he is currently a Professor. Since 2011, he has been serving as the Department Chairman. He has served as the Co-Chair or Program Chair of international conferences, such as IEEE CASE and the International Conference on Automation. In addition, he served as the TPC Member of IEEE MEMS, IEEE NEMS, and IEEE IECON. He is currently the Board Director of the Chinese Institute of Automation Engineering, the Chinese Society of Mechanical Engineers, and the ASME Taipei Chapter.

His research interests include microelectromechanical systems, high-precision micromachining, flexible sensing arrays, sensor network, parallel processing, and semiconductor devices. He is also a recipient of the Outstanding Research Award, as well as the Dr. Da-Yu Wu Memorial Award (Outstanding Young Researcher Award) of the National Science Council. He also received the NTU Outstanding Researcher Award.

Authorized licensed use limited to: Nanyang Technological University Library. Downloaded on November 14,2024 at 14:27:51 UTC from IEEE Xplore. Restrictions apply.